

Article

Optimization of the Preparation Conditions of Aluminum-Impregnated Food Waste Biochar Using RSM with an MLP and Its Application in Phosphate Removal

Jin-Kyu Kang ^{1,†} , Khonekeo Kingkhangbang ^{2,†}, Chang-Gu Lee ³ and Seong-Jik Park ^{4,*} 

¹ Institute for Environment and Energy, Pusan National University, Busan 46241, Republic of Korea; jinkyu.kang@pusan.ac.kr

² Department of Chemical Engineering, Hankyong National University, Anseong 17579, Republic of Korea; khonekeoit@yahoo.com

³ Department of Environmental and Safety Engineering, Ajou University, Suwon 16499, Republic of Korea; changgu@ajou.ac.kr

⁴ Department of Bioresources and Rural System Engineering, Hankyong National University, Anseong 17579, Republic of Korea

* Correspondence: parkseongjik@hknu.ac.kr; Tel.: +82-670-5131

† These authors contributed equally to this work.

Abstract: Phosphorus is an essential macroelement in plant growth and the human body, but excessive water enrichment with phosphorus is a global threat to water quality. To address this problem, the development of an efficient, affordable adsorbent for use in removing large amounts of phosphorus from eutrophic water is necessary. Food-waste-based adsorbents offer a sustainable solution because they utilize waste as a valuable resource. This study explored the use of food waste biochar as a novel adsorbent with additional aluminum impregnation (Al-FWB) to enhance its phosphate adsorption capacity. This study employed response surface methodology (RSM) to optimize the synthetic conditions of the Al-FWB with the highest phosphate adsorption capacity. To enhance the identification of the optimal conditions using RSM, this study employed quadratic equations and a multi-layer perceptron (MLP). The pyrolysis temperature and Al concentration significantly ($p < 0.05$) affected the adsorption capacity of the Al-FWB. The optimal conditions for the preparation of the Al-FWB were a pyrolysis temperature, duration, and Al concentration of 300 °C, 0.5 h, and 6%, respectively, based on the quadratic equation and MLP models. X-ray photoelectron spectroscopy revealed that phosphate was adsorbed on the surface of the Al-FWB via the formation of $AlPO_4$. The optimized Al-FWB (Opt-AL-FWB) removed 99.6% of the phosphate and displayed a maximum phosphate adsorption capacity of 197.8 mg/g, which is comparable to those reported in previous studies. Additionally, the phosphate adsorption capacity of the Opt-AL-FWB was independent of the pH of the solution, and the presence of 10 mM SO_4^{2-} decreased its adsorption capacity by 15.5%. The use of the Opt-AL-FWB as an adsorbent provides not only efficient phosphate removal but also green, economical food waste reusability. In summary, this study demonstrates the potential of Al-FWB as an effective, sustainable, and affordable adsorbent for use in phosphate removal from contaminated water.

Keywords: aluminum impregnation; biochar; food waste; phosphate removal; optimization; response surface methodology; multi-layer perceptron



Citation: Kang, J.-K.; Kingkhangbang, K.; Lee, C.-G.; Park, S.-J. Optimization of the Preparation Conditions of Aluminum-Impregnated Food Waste Biochar Using RSM with an MLP and Its Application in Phosphate Removal. *Water* **2023**, *15*, 2997. <https://doi.org/10.3390/w15162997>

Academic Editors: Natalija Velić, Marija Stjepanović and Nataša Jovičić

Received: 14 July 2023

Revised: 10 August 2023

Accepted: 16 August 2023

Published: 20 August 2023



Copyright: © 2023 by the authors. Licensee MDPI, Basel, Switzerland. This article is an open access article distributed under the terms and conditions of the Creative Commons Attribution (CC BY) license (<https://creativecommons.org/licenses/by/4.0/>).

1. Introduction

Phosphorus is an indispensable macroelement in plant growth and the human body [1]. It is an essential plant nutrient for growth enhancement, development, and yield and is thus applied as phosphate in soil in large quantities [2]. However, the unused phosphate derived from agricultural fertilizers from non-point and point sources enters surrounding

water bodies, causing eutrophication [3]. Phosphate pollution is a global threat because of the effects of industrial and agricultural activities and the acceleration of eutrophication in aquatic media [4]. Notably, eutrophication due to increasing algal overgrowth and oxygen depletion may threaten human health, severely endanger aquatic ecosystems, and cause effects such as the unpalatability of drinking water and declining waterway values [5]. Therefore, the remediation of phosphates in aqueous solutions is imperative because this is a growing environmental concern.

Several techniques have been developed for use in the removal of phosphate ions from aqueous solutions, including membrane [6–9] and activated sludge processing [10], struvite formation [11–13], biological treatment [14], chemical precipitation [15], and adsorption [16–18]. Among these, adsorption exhibits considerable potential in eliminating phosphate from contaminated water [19–21], offering several advantages, such as convenience, eco-friendliness, a simple design and low cost, and reusability. Several adsorbents have been studied and used to remove phosphate from water, including zeolites [22], iron oxides [23], aluminum oxides [24], and activated carbon [25]. However, several of these adsorbents exhibit undesirable adsorption properties; thus, efficient, low-cost adsorbents should be developed.

Approximately 1.3 billion metric tons of food are wasted annually, resulting in a significant amount of waste that is stored in landfills [26], thereby generating excess greenhouse gases and environmental problems, such as odors and leachates [27]. Over the years, the valorization of food waste into biochar via a circular economy has attracted the attention of environmentalists, policymakers, and researchers [28]. Biochar is a carbon-rich substance produced by pyrolyzing various biomass sources, such as agricultural waste, wood chips, algae, manure, sewage sludge, and municipal solid waste [29]. Several studies identified the potential advantages of using biochar in soil amendments, including waste management, bioenergy production [30], and water remediation [31,32].

The physicochemical properties of biochar, including its surface area, pore size distribution, and functional groups, enable its sorption properties [33]. Furthermore, the sorption characteristics of biochar are significantly influenced by modifications, and several approaches have been reported, including those based on acids, alkalis, oxidizing agents, and metal salts [4,34–38]. The preparation and modification of adsorbents with metals are simple, efficient methods of removing phosphates from water [4,39–41]. However, phosphate removal using aluminum-impregnated food-waste-based biochar (AL-FWB) is not reported, although aluminum impregnation may enhance the phosphate adsorption characteristics [42], which may vary significantly depending on the aluminum impregnation conditions. Therefore, determining the optimal synthetic conditions and preparing AL-FWB are crucial in effective phosphate adsorption. Response surface methodology (RSM) is widely used to estimate optimal conditions and should be effective in preparing AL-FWB for use in efficient phosphate adsorption.

The advantages of RSM over conventional experimental designs include the efficient exploration of the response surface, identification of the optimal conditions, analyses of interactions and nonlinear effects, statistical inference and model validation, and reduced experimental costs and time [43]. These advantages render RSM a powerful tool in optimizing experimental conditions and more effectively and efficiently realizing the desired outcomes [44]. RSM is typically applied based on a polynomial equation, but the response surfaces that may be accurately expressed solely with a polynomial model are inherently limited. A multi-layer perceptron (MLP) is an artificial neural network comprised of multiple layers of interconnected nodes known as neurons [45]. It offers advantages in optimizing experimental conditions by leveraging its nonlinear modeling capacities, automatic feature extraction, capacity to handle multivariate optimization, flexibility, adaptability to noisy data, and efficiency in parallel processing [46]. Therefore, the use of a MLP instead of the polynomial used in RSM may result in a response surface with a more flexible form, enabling a comparison or potential replacement of the optimal condition obtained using the polynomial model.

This study investigates the effectiveness of AL-FWB as an adsorbent in phosphate removal from aqueous solutions. Moreover, the main objectives are twofold: (1) optimize the AL-FWB preparation conditions using RSM with not only a quadratic equation (QE), but also MLP, and (2) investigate the sorption capacity and mechanisms of the adsorbent via property analysis and batch studies.

2. Materials and Methods

2.1. Preparation of AL-FWB

Food waste was collected as a raw material for biochar from a processing facility located in Seoul, South Korea [47]. At the facility, the food waste collected at household level was subjected to steam boiling at 150 °C followed by crushing and sieving. The food waste in this study was mainly composed of C (50.3%) along with inorganic constituents, such as Na (8.2%), Mg (5.4%), S (1.6%), Cl (15.7%), K (10.1%), and Ca (8.8%). The food waste processed in the facility was dried prior to use and then immersed in various AlCl₃ (Samchun Chemicals, Pyeongtaek, Korea) solutions (2%, 4%, or 6%). The Al-impregnated food waste was then pyrolyzed in a tube furnace at various temperatures (300, 450, or 600 °C) for various durations (0.5, 2.0, or 3.5 h). Anoxic conditions were generated by injecting N₂ gas into the tube furnace. The AL-FWB was sieved and stored in a drying oven for further use.

2.2. Application of the QE and MLP in RSM to Optimize the Preparation Conditions of AL-FWB for Use in Phosphate Removal

The concentration of the immersion solution and the temperature and duration of pyrolysis are critical factors that influence the adsorption characteristics of metal-impregnated biochar [48]. Therefore, three independent variables and their ranges were used: pyrolysis temperature (300, 450, and 600 °C) and duration (0.5, 2.0, and 3.5 h) and Al concentration (2%, 4%, and 6%) of the immersion solution. We thus used the Box-Behnken approach to design 17 sets of AL-FWB preparation conditions. Phosphate adsorption batch studies were performed to compare the phosphate removal rates of the AL-FWBs by reacting 0.3 g of AL-FWB and 30 mL of a 300 mg/L phosphate solution for 24 h at 25 °C. This specific condition was selected following preliminary tests, which exhibited significant variations in phosphate adsorption capacities among the AL-FWB samples. We did not just select the optimal AL-FWB of the 17 AL-FWBs; RSM was applied to optimize the AL-FWB preparation conditions and determine the influence of each variable on the phosphate adsorption capacity of AL-FWB. Therefore, the phosphate removal rate (%) using the AL-FWB was a response variable in RSM. Before applying RSM, the independent variables were normalized to exclude the effect of the relative magnitude of each variable using Equation S1. The original ranges and normalized values of each variable are shown in Table 1.

Table 1. Ranges of input variables and their values after normalization.

Input Variables		Normalized Value (–)		
		–1	0	1
Original value	Pyrolysis temperature (°C, X ₁)	300	450	600
	Pyrolysis duration (h, X ₂)	0.5	2.0	3.5
	Al concentration (% , X ₃)	2	4	6

The models used in RSM, i.e., the QE and MLP, were applied. The QE (Equation (1)) is optimized, and terms are selected with a backward selection algorithm using Design-Expert v13 Trial (Stat-Ease, Minneapolis, MN, USA):

$$Y = a_0 + \sum_{i=1}^3 a_i X_i + \sum_{i=1}^3 \sum_{j=i}^3 a_{i,j} X_i X_j \tag{1}$$

where Y is the phosphate removal rate predicted using the QE (–); a_0 is the constant coefficient; a_i and $a_{i,j}$ are the parametric coefficients; and X_1 , X_2 , and X_3 are the normalized pyrolysis temperature and duration and Al concentration, respectively.

Before training the MLP using the 17 datasets, the optimal hyperparameters for each dataset were identified using a grid search, and the detailed grid search conditions and results are shown in Table S1. Once the optimal hyperparameters were selected, the 17 datasets were determined to be equally crucial for training the MLP model, and thus, all 17 datasets were used for model training. The optimal synthetic conditions of the AL–FWB (Opt-AL–FWB) were determined based on RSM by selecting the conditions that were optimal in the QE and MLP models.

2.3. Characterization of Opt-AL–FWB

The surface area calculated using the Brunauer–Emmett–Teller plot was used to characterize the specific surface area of the modified FWB using a surface area analyzer (Quandrasorb SI, Quantachrome Instruments, Boynton Beach, FL, USA). Fourier-transform infrared (FTIR) spectroscopy of the food waste biochar was conducted using a Nicolet iS10 Fourier-transform infrared spectrometer (Thermo Fisher Scientific, Waltham, MA, USA). Field emission scanning electron microscopy (FE-SEM, S-4700, Hitachi, Tokyo, Japan) was employed to observe the morphologies of the Opt-AL–FWB surfaces, including pore development. Additionally, the elemental composition of the Opt-AL–FWB was quantified using an energy dispersive spectrometer (EDS) integrated with the FE-SEM. The state of the adsorbed phosphate on Opt-AL–FWB was confirmed using X-ray photoelectron spectroscopy (XPS, $h\nu = 1253.6$ eV, Sigma Probe with Al $K\alpha$ radiation, Thermo Fisher Scientific).

2.4. Batch Studies for Evaluation of Phosphate Adsorption Characteristics of Opt-AL–FWB

The comparison results of phosphate adsorption among the pre-prepared AL–FWBs informed both RSM and MLP techniques for identifying the optimal conditions for enhanced phosphate adsorption in Opt-AL–FWB. Following this optimization, Opt-AL–FWB was synthesized. To comprehensively evaluate its phosphate adsorption, batch studies were conducted to assess the characteristics of Opt-AL–FWB in phosphate removal. The studies involved varying the Opt-AL–FWB dosage, reaction time and temperature, initial phosphate concentration, initial solution pH, and the presence of coexisting anions. If no specific experimental conditions are stated, the batch studies were conducted using 0.3 g of Opt-AL–FWB and 30 mL of a 500 mg/L phosphate solution, which were added to a 50 mL conical tube and agitated at 100 rpm for 24 h at 25 °C using a shaking incubator. The reacted solutions were separated using 0.45 μm GF/C filters. The experiments were performed in triplicate, and the phosphate concentrations in the initial and reacted solutions were measured using a direct colorimetric method (United States Environmental Protection Agency (EPA) Method 365.3).

Dosage studies were performed by reacting different quantities of Opt-AL–FWB (0.05, 0.1, 0.2, 0.3, and 0.4 g) with 30 mL of the 500 mg/L phosphate solution. These studies were performed to compare the effects of the dosage on phosphate removal. Kinetic studies were conducted for 0.5, 1, 2, 3, 6, 12, and 24 h, and the initial phosphate concentrations used in the equilibrium batch studies were 10, 25, 50, 100, 300, 500, and 700 mg/L. The thermodynamic adsorption study involved using a reaction temperature of 15, 25, or 35 °C. The effect of the initial pH was examined at pH 3, 5, 7, 9, and 11 via adjustment with 0.1 M HCl and/or NaOH solutions. To assess the effects of competing anions on phosphate adsorption, Na_2SO_4 , NaHCO_3 , or NaNO_3 (Samchun Chemicals, Pyeongtaek, Korea) was added at a concentration of 1 or 10 mM.

The results of the kinetic studies were analyzed using pseudo-first-order and pseudo-second-order models (Equations (S3) and (S4)), and those of the equilibrium studies were analyzed using the Langmuir and Freundlich models (Equations (S5) and (S6)). The thermodynamic parameters were calculated using Equations (S7)–(S9), and all model

parameters were estimated via nonlinear regression using the dynamic fit Wizard function in SigmaPlot 10.0 (IBM, Armonk, NY, USA).

3. Results and Discussion

3.1. Optimization of AL-FWB Preparation for Use in Phosphate Adsorption via RSM with the QE or MLP

Utilizing Equation 1, the QE model obtained without term selection demonstrated an R^2 value of 0.929 for the 17 datasets (Table S2). When excluding terms deemed insignificant through backward selection among them, the R^2 values of the QE and MLP models were 0.904 and 0.908, respectively. Therefore, utilizing both models to determine the optimal synthetic conditions was deemed meaningful. The pair plots, sum of squares errors, and R^2 values of the 17 datasets obtained using the two models are shown in Figure S1. The optimized QE is given by Equation (2).

$$Y = 0.7142 - 0.04900X_1 + 0.02963X_3 - 0.03110X_1X_3 + 0.04737X_1^2 \quad (2)$$

Based on the QE, the optimal conditions of AL-FWB preparation are a pyrolysis temperature and Al concentration of 300 °C and 6%, respectively, and as there are no terms related to pyrolysis duration, any value between 0.5 and 3.5 h may be sufficient. The expected phosphate removal rate under these optimal conditions is 0.8713 (–). Unlike the QE, which provides several optimized conditions, the MLP identifies a single optimal synthetic condition with a pyrolysis temperature and duration and Al concentration of 300 °C, 0.5 h, and 6%, respectively. The expected response under the optimal conditions is 0.8701. The optimal conditions presented by the MLP are consistent with one of the optimal conditions presented by the QE. Opt-AL-FWB synthesized under the optimal conditions identified by the MLP was used for further study.

Figure 1 shows the response surfaces obtained using the QE and MLP, and the similarity between the response surfaces generated with the two models is confirmed. Increasing the Al concentration and decreasing the pyrolysis temperature increases phosphate removal. In contrast, the thermal decomposition time exhibits a negligible effect on the response.

The results of the analysis of variance (ANOVA) of the QE model are shown in Tables 2 and S3. The F -value (28.35) indicates that the developed regression model is significant, and the p -value (<0.0001) also indicates the validity of the optimized model. The statistical analysis reveals that the terms X_1 , X_3 , $X_1 \times X_3$, and X_1^2 are statistically significant ($p < 0.05$), indicating that pyrolysis temperature and concentration are crucial, not only individually, but also to the phosphate removal characteristics of the AL-FWB. In contrast, no pyrolysis duration-related terms are significant. The pyrolysis duration is considered sufficient even at 0.5 h (the smallest pyrolysis duration within the Box-Behnken design range), and extending the pyrolysis duration displays no effect. As presented in Table S3, an R^2 value of 0.904 for the 17 datasets suggests that the model is good for predicting the phosphate removal rate based on the evaluated experimental conditions. Therefore, the predicted R^2 value of 0.776 is consistent with the adjusted R^2 value of 0.872, confirming that the predicted values are reliable and close to the real values. An adequate precision of 18.4, which is >4 , indicates that this model is sufficient to navigate the design space [49,50].

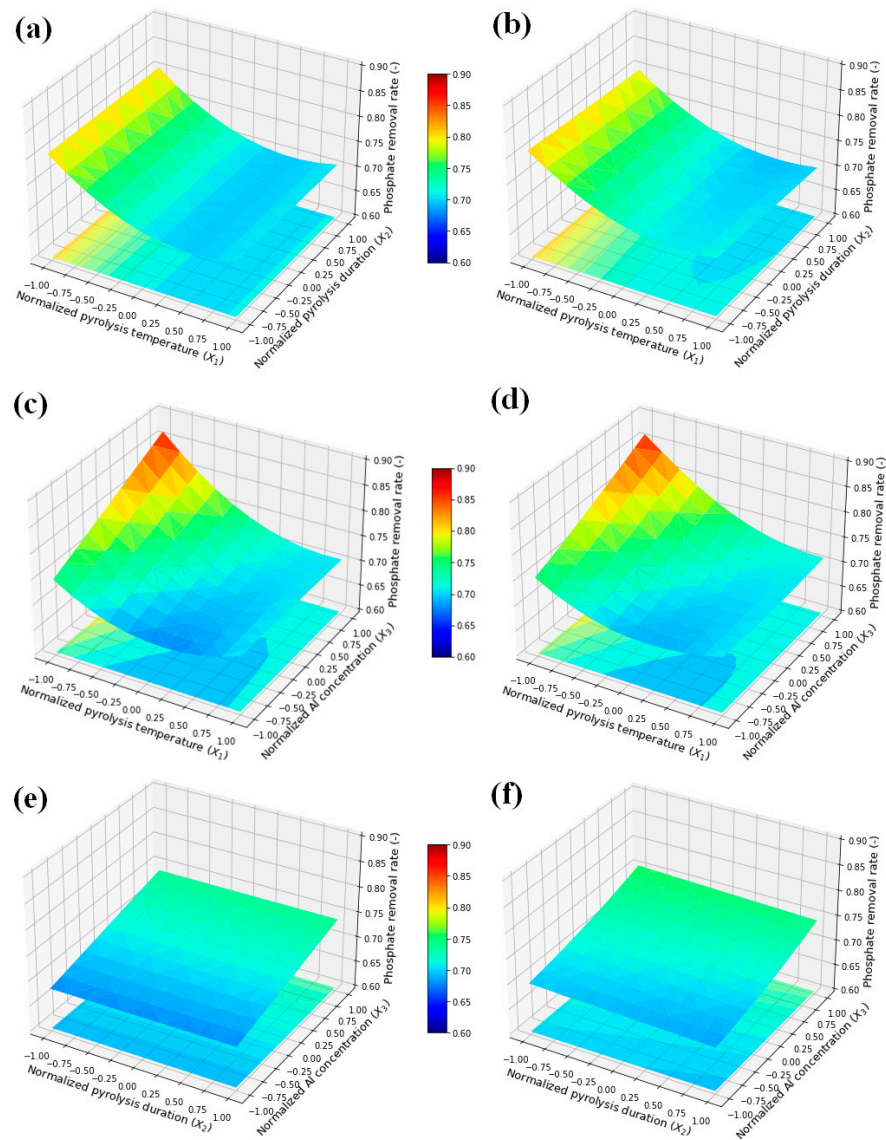


Figure 1. Response surfaces of phosphate removal rate estimated using the optimized quadratic equation (QE) and multi-layer perceptron (MLP): Effects of pyrolysis temperature and duration based on the QE (a) and MLP (b), pyrolysis temperature and Al concentration based on the QE (c) and MLP (d), and pyrolysis duration and Al concentration based on the QE (e) and MLP (f).

Table 2. Results of the analysis of variance of the optimized quadratic equation used in predicting the phosphate removal rate of AL-FWB prepared using Box–Behnken designed conditions.

Source	Sum of Squares	Degree of Freedom	Mean Square	F-Value	p-Value Prob. > F
Model	0.040	4	9.9×10^{-3}	28.35	<0.0001
X_1	0.019	1	0.019	55.01	<0.0001
X_3	7.0×10^{-3}	1	7.0×10^{-3}	20.12	0.0007
X_1X_3	3.9×10^{-3}	1	3.9×10^{-3}	11.08	0.0060
X_1^2	9.5×10^{-3}	1	9.5×10^{-3}	27.21	0.0002
Residual	4.2×10^{-3}	12	3.5×10^{-4}		
Lack of fit	4.1×10^{-3}	8	5.1×10^{-4}	21.31	0.0050
Pure Error	9.6×10^{-5}	4	2.4×10^{-5}		
Total	0.044	16			

3.2. Characteristics of Opt-AL-FWB

The FE-SEM image shows that the pores on the Opt-AL-FWB surface do not develop significantly (Figure 2a). The specific surface area and pore characteristics also indicate that the pores are not significantly developed (Table 3), potentially due to blockage via impregnation, which is also reported in other studies [51]. Several particles on the surface are aluminum or salts. Based on the elemental composition results from EDS, Opt-AL-FWB mainly comprises C and O, but Na and Cl derived from food waste and Al derived from Al impregnation are also observed (Table 3).

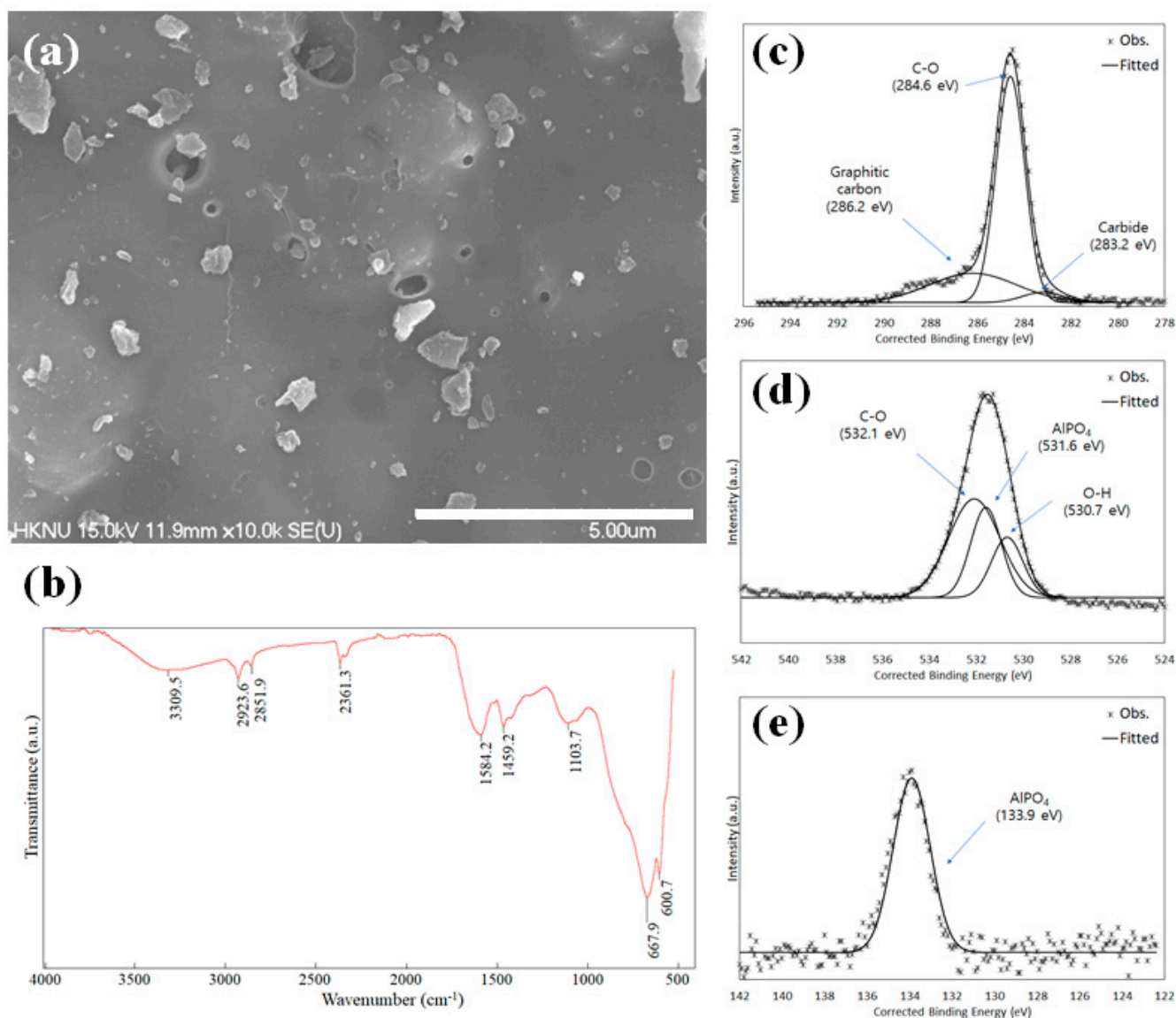


Figure 2. FE-SEM image (a) and FTIR spectrum of Opt-AL-FWB (b) and XPS spectra of phosphate-adsorbed Opt-AL-FWB: C 1s (c), O 1s (d), and P 2p (e).

Table 3. Elemental composition, specific surface area, and results of pore analysis of Opt-AL-FWB.

Adsorbents	Elements (Wt%)						Specific Surface Area and Pore Analyses		
	C	O	Al	Cl	Na	Ca	Specific Surface Area (m ² g ⁻¹)	Pore Volume (cm ³ g ⁻¹)	Average Pore Diameter (nm)
Opt-AL-FWB	42.0 ± 13.8	23.4 ± 5.5	12.1 ± 5.7	14.5 ± 6.6	4.8 ± 0.4	2.6 ± 0.3	10.4	0.031	12.1

The FTIR spectrum of Opt-AL-FWB is shown in Figure 2b with the peak at 3300 cm^{-1} ascribed to the $-\text{OH}$ stretching of water molecules [52,53]. The peaks at 2924 and 2852 cm^{-1} may be attributed to CH_2 asymmetric/symmetric stretching [54,55], and several peaks at $1600\text{--}1300\text{ cm}^{-1}$ correspond to $\text{C}=\text{C}$, $\text{C}-\text{H}$, and $\text{O}-\text{H}$ vibrations [56]. The peak at 1104 cm^{-1} is attributed to $\text{C}-\text{O}$ or skeletal $\text{C}-\text{C}$ vibrations [57,58]. Based on these peaks, Opt-AL-FWB appears to be a carbonaceous material. The broad peaks at $<700\text{ cm}^{-1}$ are due to $\text{Al}-\text{OH}$ bending [59], indicating that Al is impregnated well in Opt-AL-FWB.

Figure 2c–e show the deconvoluted XPS spectra of the phosphate-adsorbed Opt-AL-FWB. The three peaks detected for C 1s may be attributed to carbide, C–O, and graphitic carbon with respective binding energies of 283.2, 284.6, and 286.2 eV. This finding is consistent with those of previous studies in terms of biochar C 1s deconvolution [60–62]. The O 1s peaks are similarly deconvoluted into peaks representing O–H, AlPO_4 , and C–O at 530.7, 531.6, and 532.1 eV, respectively, as reported in previous studies regarding the deconvolution of the O 1s peaks of biochar by Reguyal and Sarmah [62] and Lindblad et al. [63]. The peak representing O–H in the spectrum may be due to the presence of adsorbed water or moisture [64]. In the P 2p spectrum, the P 2p peak is attributed to AlPO_4 (133.9 eV) [63], which may be formed via the precipitation of Al^{3+} from Opt-AL-FWB. At pH 7, the rate of phosphate removal via precipitation, depending on the concentration of Al (dosage = 10 g/L, initial phosphate concentration = 500 mg/L), was calculated using Visual MINTEQ (version 3.1, Swedish University of Agricultural Sciences, Uppsala, Sweden), as shown in Figure S2. When considering that the Al content of Opt-AL-FWB is 2.6 wt.%, and the batch study is conducted with a dosage of 10 g/L, the concentration of Al when all Al in Opt-AL-FWB is dissolved is approximately 0.01 M. Under these conditions, a significant portion of the phosphate generally precipitates. Notably, however, in practical applications, assuming the complete dissolution of all Al and subsequent precipitation is challenging, and thus, other adsorption mechanisms should be involved in phosphate removal.

3.3. Effect of Adsorbent Dosage

The results of the dosage studies are shown in Figure 3. The experimental results show that the phosphate removal efficiency increases from 76.8% to 99.6% as the adsorbent dosage increases from 1.7 to 6.7 g/L, whereas the phosphate adsorption capacity decreases from 230.5 to 74.7 mg/g. No significant increase in the removal efficiency is observed at dosages of $>6.7\text{ g/L}$, and the phosphate adsorption capacity is also inversely proportional to the dosage when the dosage is $>6.7\text{ g/L}$. The decrease in the phosphate adsorption capacity with increasing adsorbent dosage may be attributed to the presence of unsaturated active sites [65].

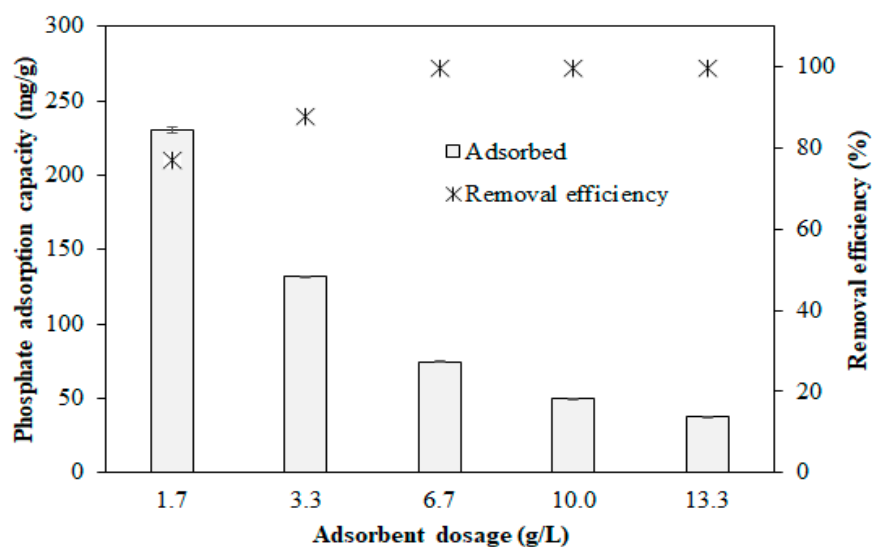


Figure 3. Effects of Opt-AL-FWB dosage on phosphate removal efficiency and adsorption capacity.

3.4. Effect of Contact Time

The results of the contact time study and fitting using the pseudo-first-order and pseudo-second-order models are shown in Figure 4 and Table S4, respectively. As shown in Figure 4, the phosphate adsorption precipitously increases to 111.7 ± 1.2 mg/g within 0.5 h and reaches 134.0 ± 0.8 mg/g at 24 h. This rapid phosphate adsorption at the beginning of the process may be attributed to its initial adsorption on the exterior surface of the biochar followed by diffusion into the pores and adsorption on the interior surface [66]. The phosphate adsorption capacities at equilibrium are 126.5 and 130.0 mg/g, according to the pseudo-first-order and pseudo-second-order models, respectively, while the R^2 of the pseudo-second-order model (0.993) is higher than that of the pseudo-first-order model (0.983). The calculated approaching equilibrium factor (R_w) from Equation (S5) was found to be 0.004. This value indicates that the adsorption characteristic curves fall within Zone 3 classification [67]. The superior fit of the experimental data to the pseudo-second-order model suggests that adsorption is dominated by chemisorption or chemical bonding between the active sites of the adsorbent and phosphate [68]. The pseudo-second-order kinetic model suggests that chemical adsorption occurs at a slower rate, thus governing the surface adsorption processes [38]. This suggests that phosphate may exchange with the hydroxyl groups on the surface of the metal oxide to form AlPO_4 , as confirmed with the XPS. This indicates a particular affinity between phosphate and the adsorbent, resulting in a high adsorption strength. However, this high affinity may render the regeneration of the adsorbent challenging [69].

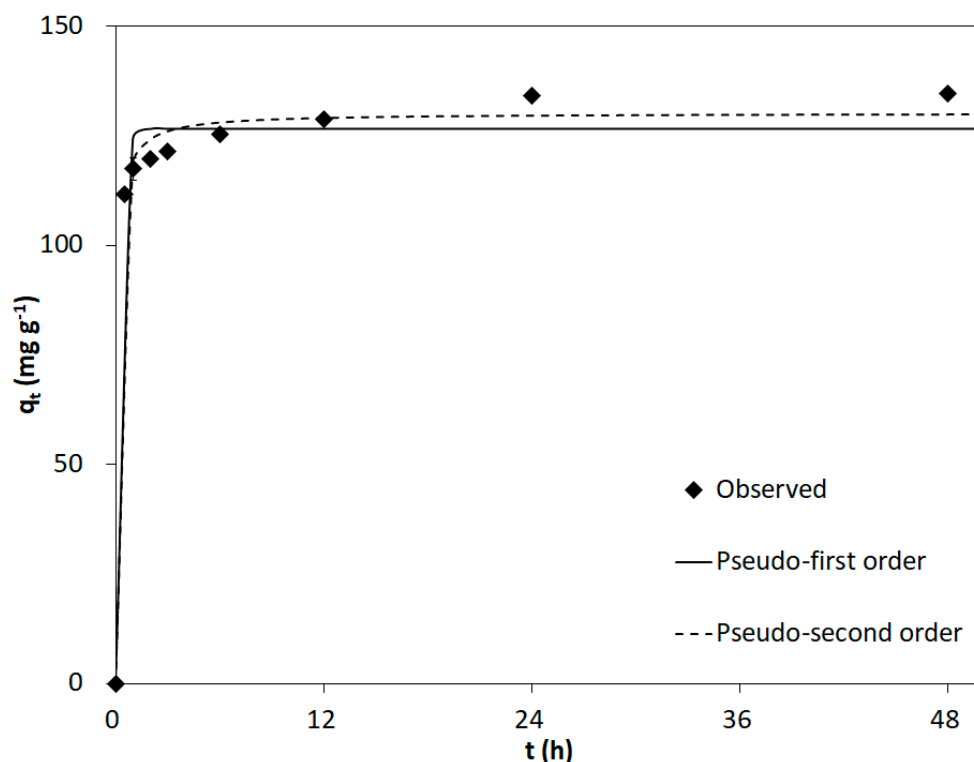


Figure 4. Kinetic adsorption data with kinetic model fitting.

3.5. Effect of Initial Phosphate Concentration

The experimental results and fitting using the Langmuir and Freundlich models are shown in Figure 5 and Table S5, and the Freundlich model is more consistent ($R^2 = 0.995$) with the observed data than the Langmuir model ($R^2 = 0.982$). The $1/n$ of the Freundlich model is 0.369, which is <0.5 , indicating that the binding between phosphate and the food waste biochar is strong with multi-layer adsorption [70,71]. The maximum phosphate adsorption capacity is 197.8 mg/g according to the Langmuir model, which is in the upper-middle level compared to that reported in previous studies of phosphate removal using

biochar (Table 4). Food waste may be pyrolyzed and used as biochar, and optimizing the conditions of Al impregnation confirms that Opt-AL-FWB may be used to effectively remove phosphate.

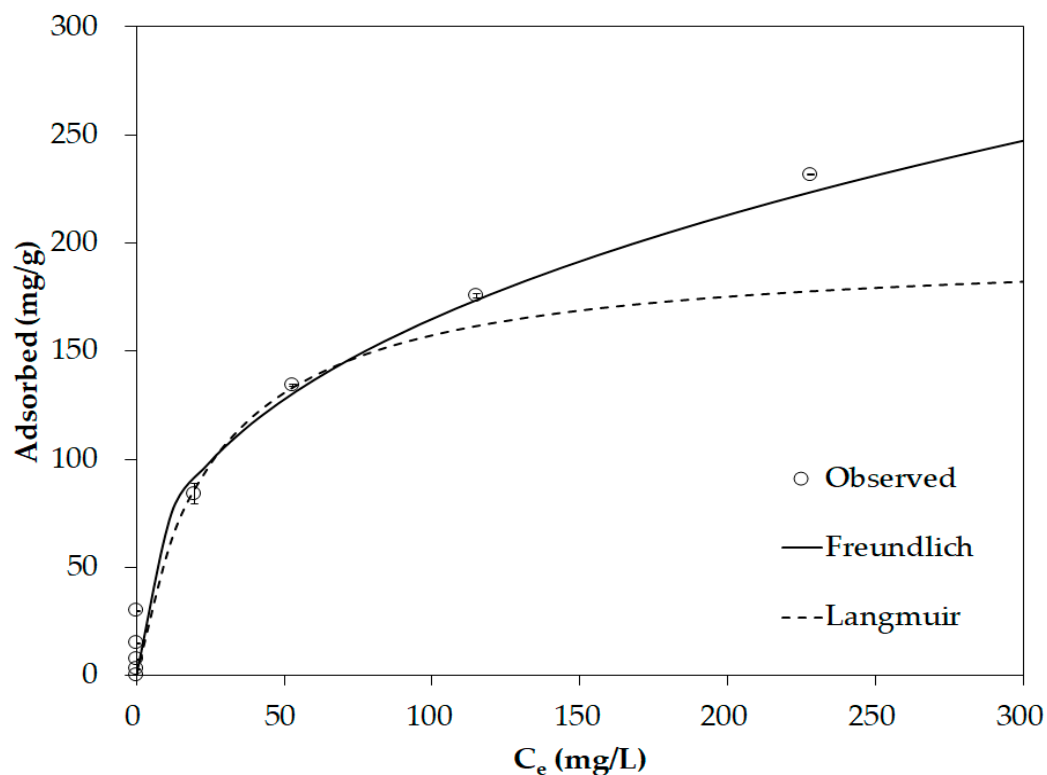


Figure 5. Equilibrium adsorption data with isotherm model fitting.

Table 4. Phosphate adsorption capacities (Q_{max}) of various biochars reported in this study and previous studies.

Feedstock	Modifier	Q_{max} (mg/g)	References
Sugar beet tailings	Not used	133.1	Yao et al. [72]
Cottonwood	Mg/Al LDH	410.0	Zhang and Gao [73]
<i>Thalia dealbata</i>	MgCl ₂ -alginate	46.6	Cui et al. [74]
<i>Laminaria japonica</i>	Calcium-alginate beads	620.7	Jung and Ahn [75]
Sugarcane harvest residue	MgO	121.3	Li, Wang, Zhou, Awasthi, Ali, Zhang, Gaston, Lahori, and Mahar [4]
Sugarcane leaves	Mg/Al LDH	81.8	Li et al. [76]
Oak	Lanthanum	46.4	Wang et al. [77]
Bamboo	Mg-Al and Mg-Fe layered double hydroxide (LDH)	172.0	Wan, Wang, Li, and Gao [41]
Food waste	Aluminum	197.8	This study

3.6. Effect of Temperature

The calculated thermodynamic results and parameters are shown in Figure 6 and Table S6. The positive change in enthalpy (ΔH°) (19.6 kJ/mol) indicates that phosphate adsorption is endothermic, and thus, adsorption increases with increasing temperature. This is due to enhanced mass transport, as the increase in temperature reduces the energy barriers of the reactions between the phosphate ions and Opt-AL-FWB [78]. The positive change in entropy (ΔS°) (83.4 J/mol·K) indicates an increase in the randomness of the system at the solid–solution interface, which facilitates phosphate adsorption on the surface of Opt-AL-FWB [79]. The negative changes in Gibbs free energy (ΔG°) (−6.0 to −4.4 kJ/mol) indicate that adsorption is spontaneous and thermodynamically favorable at all investigated temperatures [79].

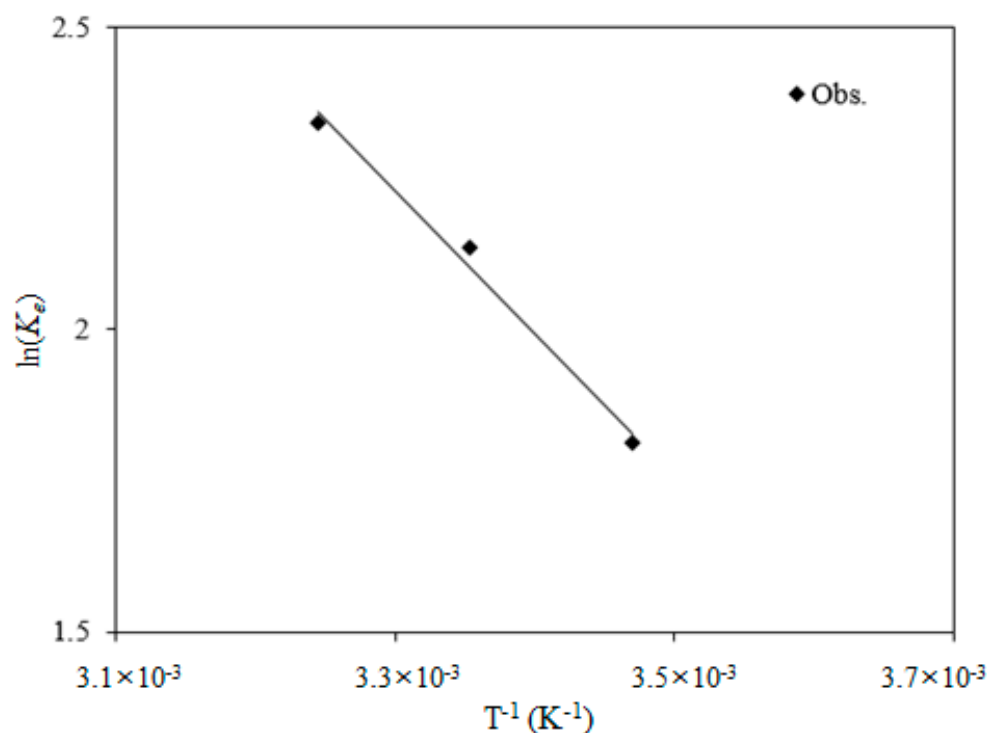


Figure 6. Thermodynamic adsorption analysis for quantifying the enthalpy and entropy.

3.7. Effect of Solution pH

The results of the pH studies and the phosphate species distributions predicted using Visual MINTEQ are shown in Figure 7a,b. At pH 3–11, the adsorption capacity is 129.0–138.7 mg/g with no drastic difference. When the solution pH is lower than the zero-charge pH of the modified AL-FWB, the biochar surface is positively charged [80]. However, phosphate mostly occurs as a neutral species (H_3PO_4) at pH 2.12, and thus, predicting phosphate adsorption via electrostatic attraction at very low pH values (<2.12) is challenging. However, as phosphate mostly occurs as $H_2PO_4^-$ at pH 3–7, the adsorption capacity is partially improved as the pH is lowered within this range, which is attributed to the enhancement of adsorption via electrostatic attraction. Nevertheless, the major species of phosphate vary depending on the pH, and the adsorption capacity is constant even at pH 11 when the surface charge should be negative, indicating that electrostatic attraction is not the main adsorption mechanism. Instead, ligand exchange between phosphate ($H_2PO_4^-$, HPO_4^{2-} , and PO_4^{3-}) and Al–OH or Al–O appears to be the main mechanism [42], which is consistent with the adsorption mechanism described above.

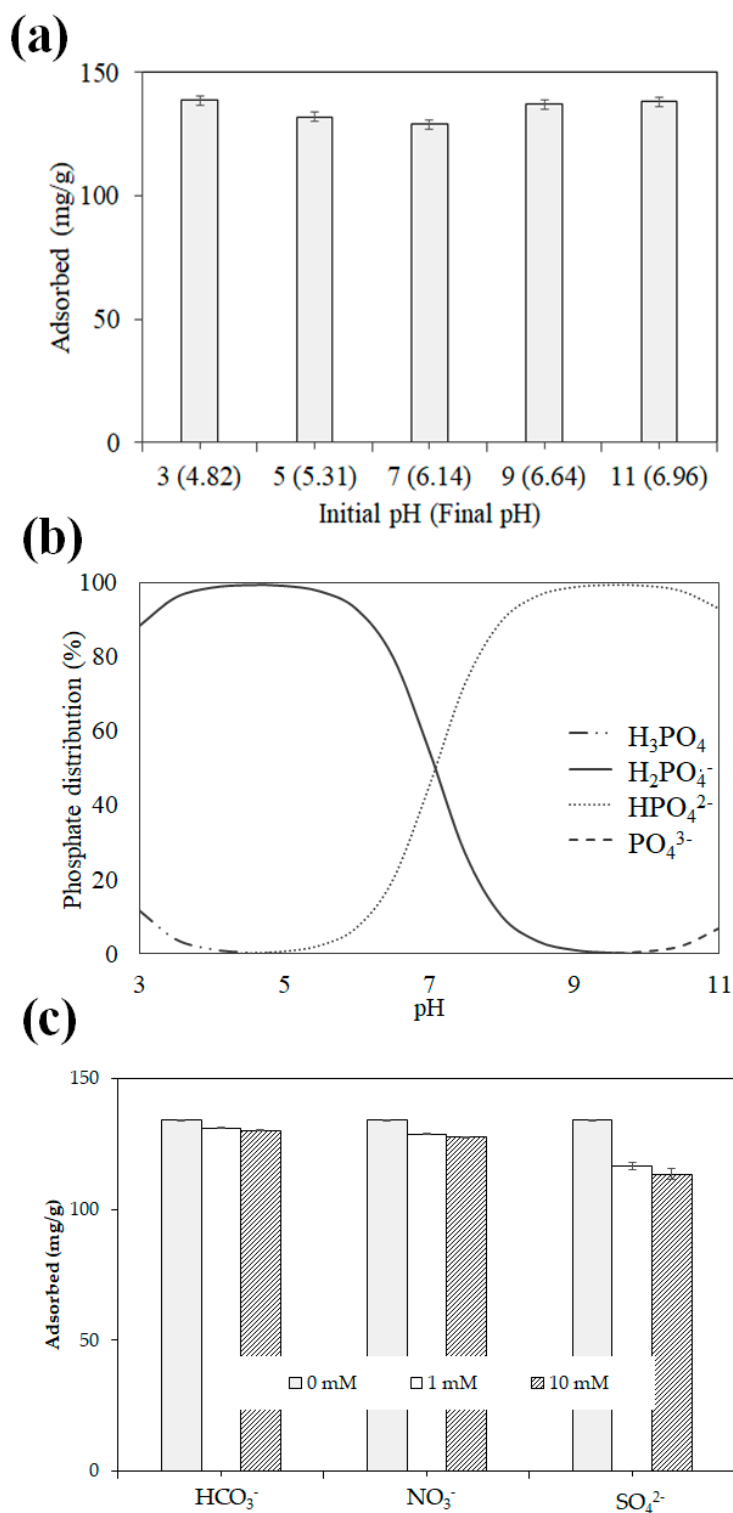


Figure 7. Effects of solution pH on the phosphate adsorption capacity of Opt-AL-FWB (a) and phosphate species distribution (as calculated using Visual MINTEQ 3.1., phosphate concentration = 500 mg/L) (b), and the effects of the competing anions on phosphate adsorption on Opt-AL-FWB (c).

3.8. Effect of Competing Anions

Figure 7c shows the results of the investigation of phosphate adsorption on Opt-AL-FWB in the presence of competing anions, such as sulfate (SO_4^{2-}), bicarbonate (HCO_3^-), or nitrate (NO_3^-). Regardless of the identity of the competing anion, increasing its concentra-

tion leads to decreased phosphate removal, as observed during the study. The inhibition differs significantly according to the identity of the competing anion in the order of $\text{HCO}_3^- < \text{NO}_3^- < \text{SO}_4^{2-}$. In the absence of oxide anions, the adsorption capacity is 134.1 mg/g, but in the presence of HCO_3^- , NO_3^- , or SO_4^{2-} at a concentration of 10 mM, the adsorption capacity decreases to 130.2, 127.7, or 113.4 mg/g, respectively. The inhibition of phosphate adsorption by SO_4^{2-} , which exhibits the highest valence among those of the competing anions, may be an ion-exchange reaction, which may be one of the mechanisms of phosphate adsorption on the material [42,68]. However, the adsorption capacity decreases by only 15.5% even when 10 mM SO_4^{2-} is present, which may be because ligand exchange remains the main adsorption mechanism.

4. Conclusions

The Box–Behnken design was employed to prepare AL–FWB and optimize the preparation conditions to yield the maximum phosphate adsorption capacity. By applying RSM with a QE and a MLP to the phosphate adsorption capacities of various AL–FWBs, the optimal conditions were obtained to ensure the maximum phosphate removal in an aqueous solution. The ANOVA revealed that the pyrolysis temperature and Al concentration significantly affected the phosphate removal characteristics, whereas the pyrolysis duration was not a factor after 0.5 h. Both the QE and MLP indicated that the optimal preparation conditions for Opt-AL–FWB were a pyrolysis temperature and duration of 300 °C and 0.5 h along with an Al concentration of 6%. Opt-AL–FWB demonstrated a remarkable maximum sorption capacity of 197.75 mg/g, as per the Langmuir model. The optimal fit of the pseudo-second-order kinetics indicated that phosphate was adsorbed via chemical bonding between the phosphate and active sites. The results of property analysis, such as those of pH and competition studies and the XPS spectra, indicated that phosphate adsorption on Opt-AL–FWB could be partially caused by electrostatic attraction but mostly caused by ligand exchange. Therefore, the use of Opt-AL–FWB as an adsorbent provides not only efficient phosphate removal but also green, economical food waste reusability. This may provide valuable data for engineers for use in preparing modified biochar, expanding biochar technology to manage waste biomass, and mitigating environmental pollution to maintain sustainable environments.

Supplementary Materials: The following supporting information can be downloaded at: <https://www.mdpi.com/article/10.3390/w15162997/s1>. References [81–87] are cited in the Supplementary Materials.

Author Contributions: J.-K.K.: Writing original draft, Data analysis; K.K.: Writing original draft; Experiment; C.-G.L.: Writing—review and editing; S.-J.P.: Conceptualization, Writing—review and editing, Supervision, Funding acquisition. All authors have read and agreed to the published version of the manuscript.

Funding: This work was supported by Korea Forest Service (Korea Forestry Promotion Institute) through an R&D program for Forest Science Technology (Project No. 2023483D10-2325-AA01). This research was also supported by Basic Science Research Program through the National Research Foundation of Korea (NRF) funded by the Ministry of Education (NRF-2021R1A6A1A03039572).

Institutional Review Board Statement: Not applicable.

Informed Consent Statement: Not applicable.

Data Availability Statement: The datasets used and/or analyzed during this study are available from the corresponding author upon reasonable request.

Conflicts of Interest: The authors declare no conflict of interest.

References

1. Hu, F.; Wang, M.; Peng, X.; Qiu, F.; Zhang, T.; Dai, H.; Liu, Z.; Cao, Z. High-efficient adsorption of phosphates from water by hierarchical CuAl/biomass carbon fiber layered double hydroxide. *Colloids Surf. A* **2018**, *555*, 314–323. [[CrossRef](#)]
2. Veni, D.K.; Kannan, P.; Edison, T.N.J.I.; Senthilkumar, A. Biochar from green waste for phosphate removal with subsequent disposal. *Waste Manag.* **2017**, *68*, 752–759. [[CrossRef](#)] [[PubMed](#)]

3. Yao, Y.; Gao, B.; Chen, J.; Yang, L. Engineered biochar reclaiming phosphate from aqueous solutions: Mechanisms and potential application as a slow-release fertilizer. *Environ. Sci. Technol.* **2013**, *47*, 8700–8708. [[CrossRef](#)] [[PubMed](#)]
4. Li, R.; Wang, J.J.; Zhou, B.; Awasthi, M.K.; Ali, A.; Zhang, Z.; Gaston, L.A.; Lahori, A.H.; Mahar, A. Enhancing phosphate adsorption by Mg/Al layered double hydroxide functionalized biochar with different Mg/Al ratios. *Sci. Total Environ.* **2016**, *559*, 121–129. [[CrossRef](#)]
5. Wu, D.; Yan, H.; Shang, M.; Shan, K.; Wang, G. Water eutrophication evaluation based on semi-supervised classification: A case study in Three Gorges Reservoir. *Ecol. Indic.* **2017**, *81*, 362–372. [[CrossRef](#)]
6. Jiang, J.; Kim, D.I.; Dorji, P.; Phuntsho, S.; Hong, S.; Shon, H.K. Phosphorus removal mechanisms from domestic wastewater by membrane capacitive deionization and system optimization for enhanced phosphate removal. *Process Saf. Environ. Prot.* **2019**, *126*, 44–52. [[CrossRef](#)]
7. Park, J.-H.; Kang, H.-J.; Kim, H.-S.; Wells, G.F.; Park, H.-D. Effects of alkali-treated sludge supplementation for enhanced biological phosphorus removal in a membrane bioreactor. *Fuel* **2019**, *254*, 115588. [[CrossRef](#)]
8. Pradhan, S.K.; Mikola, A.; Heinonen-Tanski, H.; Vahala, R. Recovery of nitrogen and phosphorus from human urine using membrane and precipitation process. *J. Environ. Manag.* **2019**, *247*, 596–602. [[CrossRef](#)]
9. Manawi, Y.; Hussien, M.; Buekenhoudt, A.; Zekri, A.; Al-Sulaiti, H.; Lawler, J.; Kochkodan, V. New ceramic membrane for Phosphate and oil removal. *J. Environ. Chem. Eng.* **2022**, *10*, 106916. [[CrossRef](#)]
10. Ge, J.; Meng, X.; Song, Y.; Terracciano, A. Effect of phosphate releasing in activated sludge on phosphorus removal from municipal wastewater. *J. Environ. Sci.* **2018**, *67*, 216–223. [[CrossRef](#)]
11. Wang, Z.; Zhang, J.; Guan, X.; She, L.; Xiang, P.; Xia, S.; Zhang, Z. Bioelectrochemical acidolysis of magnesia to induce struvite crystallization for recovering phosphorus from aqueous solution. *J. Environ. Sci.* **2019**, *85*, 119–128. [[CrossRef](#)]
12. Lu, Z.; Zhang, K.; Liu, F.; Gao, X.; Zhai, Z.; Li, J.; Du, L. Simultaneous recovery of ammonium and phosphate from aqueous solutions using Mg/Fe modified NaY zeolite: Integration between adsorption and struvite precipitation. *Sep. Purif. Technol.* **2022**, *299*, 121713. [[CrossRef](#)]
13. Mavhungu, A.; Foteinis, S.; Mbaya, R.; Masindi, V.; Kortidis, I.; Mpenyana-Monyatsi, L.; Chatzisyneon, E. Environmental sustainability of municipal wastewater treatment through struvite precipitation: Influence of operational parameters. *J. Clean. Prod.* **2021**, *285*, 124856. [[CrossRef](#)]
14. Vikrant, K.; Kim, K.-H.; Ok, Y.S.; Tsang, D.C.W.; Tsang, Y.F.; Giri, B.S.; Singh, R.S. Engineered/designer biochar for the removal of phosphate in water and wastewater. *Sci. Total Environ.* **2018**, *616–617*, 1242–1260. [[CrossRef](#)]
15. Cichy, B.; Kuźdzał, E.; Krztoń, H. Phosphorus recovery from acidic wastewater by hydroxyapatite precipitation. *J. Environ. Manag.* **2019**, *232*, 421–427. [[CrossRef](#)]
16. Zhang, X.; Lin, X.; He, Y.; Chen, Y.; Zhou, J.; Luo, X. Adsorption of phosphorus from slaughterhouse wastewater by carboxymethyl konjac glucomannan loaded with lanthanum. *Int. J. Biol. Macromol.* **2018**, *119*, 105–115. [[CrossRef](#)]
17. Peng, G.; Jiang, S.; Wang, Y.; Zhang, Q.; Cao, Y.; Sun, Y.; Zhang, W.; Wang, L. Synthesis of Mn/Al double oxygen biochar from dewatered sludge for enhancing phosphate removal. *J. Clean. Prod.* **2020**, *251*, 119725. [[CrossRef](#)]
18. Jung, K.-W.; Hwang, M.-J.; Jeong, T.-U.; Ahn, K.-H. A novel approach for preparation of modified-biochar derived from marine macroalgae: Dual purpose electro-modification for improvement of surface area and metal impregnation. *Bioresour. Technol.* **2015**, *191*, 342–345. [[CrossRef](#)] [[PubMed](#)]
19. Park, J.H.; Jung, D.I. Removal of total phosphorus (TP) from municipal wastewater using loess. *Desalination* **2011**, *269*, 104–110. [[CrossRef](#)]
20. Lee, J.-I.; Jadamba, C.; Yoo, S.-C.; Lee, C.-G.; Shin, M.-C.; Lee, J.; Park, S.-J. Cycling of phosphorus from wastewater to fertilizer using wood ash after energy production. *Chemosphere* **2023**, *336*, 139191. [[CrossRef](#)] [[PubMed](#)]
21. Lee, J.-I.; Jadamba, C.; Yoo, S.-C.; Lee, C.-G.; Park, S.-J. Value-added application of cattle manure bottom ash for phosphorus recovery from water and replenishment in soil. *J. Environ. Manag.* **2023**, *339*, 117891. [[CrossRef](#)] [[PubMed](#)]
22. Onyango, M.S.; Kuchar, D.; Kubota, M.; Matsuda, H. Adsorptive Removal of Phosphate Ions from Aqueous Solution Using Synthetic Zeolite. *Ind. Eng. Chem. Res.* **2007**, *46*, 894–900. [[CrossRef](#)]
23. Lalley, J.; Han, C.; Li, X.; Dionysiou, D.D.; Nadagouda, M.N. Phosphate adsorption using modified iron oxide-based sorbents in lake water: Kinetics, equilibrium, and column tests. *Chem. Eng. J.* **2016**, *284*, 1386–1396. [[CrossRef](#)]
24. Georgantas, D.A.; Grigoropoulou, H.P. Orthophosphate and metaphosphate ion removal from aqueous solution using alum and aluminum hydroxide. *J. Colloid Interf. Sci.* **2007**, *315*, 70–79. [[CrossRef](#)]
25. Suresh Kumar, P.; Prot, T.; Korving, L.; Keesman, K.J.; Dugulan, I.; van Loosdrecht, M.C.M.; Witkamp, G.-J. Effect of pore size distribution on iron oxide coated granular activated carbons for phosphate adsorption—Importance of mesopores. *Chem. Eng. J.* **2017**, *326*, 231–239. [[CrossRef](#)]
26. Ranganathan, S.; Dutta, S.; Moses, J.A.; Anandharamkrishnan, C. Utilization of food waste streams for the production of biopolymers. *Heliyon* **2020**, *6*, e04891. [[CrossRef](#)]
27. Morone, P.; Koutinas, A.; Gathergood, N.; Arshadi, M.; Matharu, A. Food waste: Challenges and opportunities for enhancing the emerging bio-economy. *J. Clean. Prod.* **2019**, *221*, 10–16. [[CrossRef](#)]
28. Food and Agriculture Organization of the United Nations. Food Wastage Footprint Full-Cost Accounting. 2014. Available online: <https://www.fao.org/documents/card/en?details=5e7c4154-2b97-4ea5-83a7-be9604925a24%2f> (accessed on 15 August 2023).

29. Li, L.; Zou, D.; Xiao, Z.; Zeng, X.; Zhang, L.; Jiang, L.; Wang, A.; Ge, D.; Zhang, G.; Liu, F. Biochar as a sorbent for emerging contaminants enables improvements in waste management and sustainable resource use. *J. Clean. Prod.* **2019**, *210*, 1324–1342. [[CrossRef](#)]
30. Masebinu, S.O.; Akinlabi, E.T.; Muzenda, E.; Aboyade, A.O. A review of biochar properties and their roles in mitigating challenges with anaerobic digestion. *Renew. Sustain. Energy Rev.* **2019**, *103*, 291–307. [[CrossRef](#)]
31. Melia, P.M.; Busquets, R.; Hooda, P.S.; Cundy, A.B.; Sohi, S.P. Driving forces and barriers in the removal of phosphorus from water using crop residue, wood and sewage sludge derived biochars. *Sci. Total Environ.* **2019**, *675*, 623–631. [[CrossRef](#)]
32. Novais, S.V.; Zenero, M.D.O.; Barreto, M.S.C.; Montes, C.R.; Cerri, C.E.P. Phosphorus removal from eutrophic water using modified biochar. *Sci. Total Environ.* **2018**, *633*, 825–835. [[CrossRef](#)] [[PubMed](#)]
33. Wang, J.; Wang, S. Preparation, modification and environmental application of biochar: A review. *J. Clean. Prod.* **2019**, *227*, 1002–1022. [[CrossRef](#)]
34. Rajapaksha, A.U.; Chen, S.S.; Tsang, D.C.; Zhang, M.; Vithanage, M.; Mandal, S.; Gao, B.; Bolan, N.S.; Ok, Y.S. Engineered/designer biochar for contaminant removal/immobilization from soil and water: Potential and implication of biochar modification. *Chemosphere* **2016**, *148*, 276–291. [[CrossRef](#)]
35. Huff, M.D.; Lee, J.W. Biochar-surface oxygenation with hydrogen peroxide. *J. Environ. Manag.* **2016**, *165*, 17–21. [[CrossRef](#)]
36. Jin, H.; Capareda, S.; Chang, Z.; Gao, J.; Xu, Y.; Zhang, J. Biochar pyrolytically produced from municipal solid wastes for aqueous As (V) removal: Adsorption property and its improvement with KOH activation. *Bioresour. Technol.* **2014**, *169*, 622–629. [[CrossRef](#)]
37. Liang, J.; Li, X.; Yu, Z.; Zeng, G.; Luo, Y.; Jiang, L.; Yang, Z.; Qian, Y.; Wu, H. Amorphous MnO₂ modified biochar derived from aerobically composted swine manure for adsorption of Pb (II) and Cd (II). *ACS Sustain. Chem. Eng.* **2017**, *5*, 5049–5058. [[CrossRef](#)]
38. Sadegh, N.; Haddadi, H.; Sadegh, F.; Asfaram, A. Recent advances and perspectives of tannin-based adsorbents for wastewater pollutants elimination: A review. *Environ. Nanotechnol. Monit. Manag.* **2023**, *19*, 100763. [[CrossRef](#)]
39. Liu, X.; Shen, F.; Qi, X. Adsorption recovery of phosphate from aqueous solution by CaO-biochar composites prepared from eggshell and rice straw. *Sci. Total Environ.* **2019**, *666*, 694–702. [[CrossRef](#)]
40. Saadat, S.; Raei, E.; Talebbeydokhti, N. Enhanced removal of phosphate from aqueous solutions using a modified sludge derived biochar: Comparative study of various modifying cations and RSM based optimization of pyrolysis parameters. *J. Environ. Manag.* **2018**, *225*, 75–83. [[CrossRef](#)]
41. Wan, S.; Wang, S.; Li, Y.; Gao, B. Functionalizing biochar with Mg–Al and Mg–Fe layered double hydroxides for removal of phosphate from aqueous solutions. *J. Ind. Eng. Chem.* **2017**, *47*, 246–253. [[CrossRef](#)]
42. Liu, R.; Shen, J.; He, X.; Chi, L.; Wang, X. Efficient macroporous adsorbent for phosphate removal based on hydrate aluminum-functionalized melamine sponge. *Chem. Eng. J.* **2020**, *421*, 127848. [[CrossRef](#)]
43. Djimtoingar, S.S.; Derkyi, N.S.A.; Kuranchie, F.A.; Yankyera, J.K. A review of response surface methodology for biogas process optimization. *Cogent Eng.* **2022**, *9*, 2115283. [[CrossRef](#)]
44. Ghelich, R.; Jahannama, M.R.; Abdizadeh, H.; Torknik, F.S.; Vaezi, M.R. Central composite design (CCD)-Response surface methodology (RSM) of effective electrospinning parameters on PVP-B-Hf hybrid nanofibrous composites for synthesis of HfB₂-based composite nanofibers. *Compos. B Eng.* **2019**, *166*, 527–541. [[CrossRef](#)]
45. Pinkus, A. Approximation theory of the MLP model in neural networks. *Acta Numer.* **1999**, *8*, 143–195. [[CrossRef](#)]
46. Bishop, C.M. *Neural Networks for Pattern Recognition*; Oxford University Press: Oxford, UK, 1995.
47. Lyonga, F.N.; Hong, S.-H.; Cho, E.-J.; Kang, J.-K.; Lee, C.-G.; Park, S.-J. As(III) adsorption onto Fe-impregnated food waste biochar: Experimental investigation, modeling, and optimization using response surface methodology. *Environ. Geochem. Health* **2021**, *43*, 3303–3321. [[CrossRef](#)] [[PubMed](#)]
48. Kang, J.-K.; Seo, E.-J.; Lee, C.-G.; Park, S.-J. Fe-loaded biochar obtained from food waste for enhanced phosphate adsorption and its adsorption mechanism study via spectroscopic and experimental approach. *J. Environ. Chem. Eng.* **2021**, *9*, 105751. [[CrossRef](#)]
49. Jung, K.-W.; Jeong, T.-U.; Kang, H.-J.; Chang, J.-S.; Ahn, K.-H. Preparation of modified-biochar from *Laminaria japonica*: Simultaneous optimization of aluminum electrode-based electro-modification and pyrolysis processes and its application for phosphate removal. *Bioresour. Technol.* **2016**, *214*, 548–557. [[CrossRef](#)]
50. Arabkhani, P.; Saeedi, N.; Sadeghi, H.; Nouripour-Sisakht, S.; Gharaghani, M.; Asfaram, A. Plant extracts-mediated green synthesis of zinc oxide/carbon nanofiber nanocomposites with highly efficient photocatalytic and antimicrobial properties for wastewater treatment. *J. Water Process Eng.* **2023**, *54*, 104020. [[CrossRef](#)]
51. Bailon, M.X.; Chaudhary, D.K.; Jeon, C.; Ok, Y.S.; Hong, Y. Impact of sulfur-impregnated biochar amendment on microbial communities and mercury methylation in contaminated sediment. *J. Hazard. Mater.* **2022**, *438*, 129464. [[CrossRef](#)]
52. Wang, H.; Wang, S.; Chen, Z.; Zhou, X.; Wang, J.; Chen, Z. Engineered biochar with anisotropic layered double hydroxide nanosheets to simultaneously and efficiently capture Pb²⁺ and CrO₄²⁻ from electroplating wastewater. *Bioresour. Technol.* **2020**, *306*, 123118. [[CrossRef](#)]
53. Mojet, B.L.; Ebbesen, S.D.; Lefferts, L. Light at the interface: The potential of attenuated total reflection infrared spectroscopy for understanding heterogeneous catalysis in water. *Chem. Soc. Rev.* **2010**, *39*, 4643. [[CrossRef](#)] [[PubMed](#)]
54. Li, Q.; Liang, W.; Liu, F.; Wang, G.; Wan, J.; Zhang, W.; Peng, C.; Yang, J. Simultaneous immobilization of arsenic, lead and cadmium by magnesium-aluminum modified biochar in mining soil. *J. Environ. Manag.* **2022**, *310*, 114792. [[CrossRef](#)] [[PubMed](#)]
55. Simons, W.W. *The Sadtler Handbook of Infrared Spectra*; Sadtler Research Laboratories: Philadelphia, PA, USA, 1978.
56. Socrates, G. *Infrared and Raman Characteristic Group Frequencies: Tables and Charts*, 3rd ed.; John Wiley & Sons: London, UK, 2001.

57. Coates, J. Interpretation of Infrared Spectra, A Practical Approach. In *Encyclopedia of Analytical Chemistry*; John Wiley & Sons: Hoboken, NJ, USA, 2006.
58. Peng, C.; Gong, K.; Li, Q.; Liang, W.; Song, H.; Liu, F.; Yang, J.; Zhang, W. Simultaneous immobilization of arsenic, lead, and cadmium in soil by magnesium-aluminum modified biochar: Influences of organic acids, aging, and rainfall. *Chemosphere* **2023**, *313*, 137453. [[CrossRef](#)] [[PubMed](#)]
59. Birnin-Yauri, U.A.; Glasser, F.P. Friedel's salt, $\text{Ca}_2\text{Al}(\text{OH})_6(\text{Cl},\text{OH})\cdot 2\text{H}_2\text{O}$: Its solid solutions and their role in chloride binding. *Cem. Concr. Res.* **1998**, *28*, 1713–1723. [[CrossRef](#)]
60. Terzyk, A.P. The influence of activated carbon surface chemical composition on the adsorption of acetaminophen (paracetamol) in vitro: Part II. TG, FTIR, and XPS analysis of carbons and the temperature dependence of adsorption kinetics at the neutral pH. *Colloids Surf. A* **2001**, *177*, 23–45. [[CrossRef](#)]
61. Puziy, A.M.; Poddubnaya, O.I.; Socha, R.P.; Gurgul, J.; Wisniewski, M. XPS and NMR studies of phosphoric acid activated carbons. *Carbon* **2008**, *46*, 2113–2123. [[CrossRef](#)]
62. Reguyal, F.; Sarmah, A.K. Adsorption of sulfamethoxazole by magnetic biochar: Effects of pH, ionic strength, natural organic matter and 17α -ethinylestradiol. *Sci. Total Environ.* **2018**, *628–629*, 722–730. [[CrossRef](#)]
63. Lindblad, T.; Rebenstorf, B.; Yan, Z.-G.; Andersson, S.L.T. Characterization of vanadia supported on amorphous AlPO_4 and its properties for oxidative dehydrogenation of propane. *Appl. Catal. A Gen.* **1994**, *112*, 187–208. [[CrossRef](#)]
64. Rosenthal, D.; Ruta, M.; Schlögl, R.; Kiwi-Minsker, L. Combined XPS and TPD study of oxygen-functionalized carbon nanofibers grown on sintered metal fibers. *Carbon* **2010**, *48*, 1835–1843. [[CrossRef](#)]
65. Padmavathy, K.; Madhu, G.; Haseena, P. A study on effects of pH, adsorbent dosage, time, initial concentration and adsorption isotherm study for the removal of hexavalent chromium (Cr (VI)) from wastewater by magnetite nanoparticles. *Proc. Technol.* **2016**, *24*, 585–594. [[CrossRef](#)]
66. Chen, W.; Wei, R.; Yang, L.; Yang, Y.; Li, G.; Ni, J. Characteristics of wood-derived biochars produced at different temperatures before and after deashing: Their different potential advantages in environmental applications. *Sci. Total Environ.* **2019**, *651*, 2762–2771. [[CrossRef](#)] [[PubMed](#)]
67. Wu, F.-C.; Tseng, R.-L.; Huang, S.-C.; Juang, R.-S. Characteristics of pseudo-second-order kinetic model for liquid-phase adsorption: A mini-review. *Chem. Eng. J.* **2009**, *151*, 1–9. [[CrossRef](#)]
68. Kim, M.-J.; Lee, J.-H.; Lee, C.-G.; Park, S.-J. Thermal treatment of attapulgite for phosphate removal: A cheap and natural adsorbent with high adsorption capacity. *Desalin. Water Treat.* **2018**, *114*, 174–184. [[CrossRef](#)]
69. Yang, J.; Zhou, L.; Zhao, L.; Zhang, H.; Yin, J.; Wei, G.; Qian, K.; Wang, Y.; Yu, C. A designed nanoporous material for phosphate removal with high efficiency. *J. Mater. Chem.* **2011**, *21*, 2489–2494. [[CrossRef](#)]
70. Edzwald, J.; Association, A.W.W. *Water Quality & Treatment: A Handbook on Drinking Water*; McGraw-Hill Education: Newyork, USA, 2011.
71. Belhachemi, M. Chapter 14—Adsorption of organic compounds on activated carbons. In *Sorbents Materials for Controlling Environmental Pollution*, Núñez-Delgado, A., Ed.; Elsevier: Amsterdam, The Netherlands, 2021; pp. 355–385.
72. Yao, Y.; Gao, B.; Inyang, M.; Zimmerman, A.R.; Cao, X.; Pullammanappallil, P.; Yang, L. Removal of phosphate from aqueous solution by biochar derived from anaerobically digested sugar beet tailings. *J. Hazard. Mater.* **2011**, *190*, 501–507. [[CrossRef](#)] [[PubMed](#)]
73. Zhang, M.; Gao, B. Removal of arsenic, methylene blue, and phosphate by biochar/ AlOOH nanocomposite. *Chem. Eng. J.* **2013**, *226*, 286–292. [[CrossRef](#)]
74. Cui, X.; Dai, X.; Khan, K.Y.; Li, T.; Yang, X.; He, Z. Removal of phosphate from aqueous solution using magnesium-alginate/chitosan modified biochar microspheres derived from *Thalia dealbata*. *Bioresour. Technol.* **2016**, *218*, 1123–1132. [[CrossRef](#)]
75. Jung, K.-W.; Ahn, K.-H. Fabrication of porosity-enhanced MgO /biochar for removal of phosphate from aqueous solution: Application of a novel combined electrochemical modification method. *Bioresour. Technol.* **2016**, *200*, 1029–1032. [[CrossRef](#)]
76. Li, R.; Wang, J.J.; Zhou, B.; Awasthi, M.K.; Ali, A.; Zhang, Z.; Lahori, A.H.; Mahar, A. Recovery of phosphate from aqueous solution by magnesium oxide decorated magnetic biochar and its potential as phosphate-based fertilizer substitute. *Bioresour. Technol.* **2016**, *215*, 209–214. [[CrossRef](#)]
77. Wang, Z.; Shen, D.; Shen, F.; Li, T. Phosphate adsorption on lanthanum loaded biochar. *Chemosphere* **2016**, *150*, 1–7. [[CrossRef](#)]
78. Do, D.D. *Adsorption Analysis: Equilibria and Kinetics*; Imperial College Press London: London, UK, 1998; Volume 2.
79. Rashid, M.; Price, N.T.; Gracia Pinilla, M.Á.; O'Shea, K.E. Effective removal of phosphate from aqueous solution using humic acid coated magnetite nanoparticles. *Water Res.* **2017**, *123*, 353–360. [[CrossRef](#)] [[PubMed](#)]
80. Milagres, J.L.; Bellato, C.R.; Vieira, R.S.; Ferreira, S.O.; Reis, C. Preparation and evaluation of the Ca-Al layered double hydroxide for removal of copper(II), nickel(II), chromium(VI) and phosphate from aqueous solution. *J. Environ. Chem. Eng.* **2017**, *5*, 5469–5480. [[CrossRef](#)]
81. Ho, Y.S.; McKay, G. Kinetic Model for Lead(II) Sorption on to Peat. *Adsorpt. Sci. Technol.* **1998**, *16*, 243–255. [[CrossRef](#)]
82. Lagergren, S.K. About the theory of so-called adsorption of soluble substances. *Sven. Vetenskapsakad. Handlingar* **1898**, *24*, 1–39.
83. Freundlich, H. Über die Adsorption in Lösungen. *Z. Phys. Chem.* **1907**, *57U*, 385–470. [[CrossRef](#)]
84. Langmuir, I. The constitution and fundamental properties of solids and liquids. Part I. solids. *J. Am. Chem. Soc.* **1916**, *38*, 2221–2295. [[CrossRef](#)]

85. Kim, J.-H.; Kang, J.-K.; Lee, S.-C.; Kim, S.-B. Immobilization of layered double hydroxide in poly(vinylidene fluoride)/poly(vinyl alcohol) polymer matrices to synthesize bead-type adsorbents for phosphate removal from natural water. *Appl. Clay Sci.* **2019**, *170*, 1–12. [[CrossRef](#)]
86. Lima, E.C.; Gomes, A.A.; Tran, H.N. Comparison of the nonlinear and linear forms of the van't Hoff equation for calculation of adsorption thermodynamic parameters (ΔS° and ΔH°). *J. Mol. Liq.* **2020**, *311*, 113315. [[CrossRef](#)]
87. Wang, L. Application of activated carbon derived from 'waste' bamboo culms for the adsorption of azo disperse dye: Kinetic, equilibrium and thermodynamic studies. *J. Environ. Manag.* **2012**, *102*, 79–87. [[CrossRef](#)]

Disclaimer/Publisher's Note: The statements, opinions and data contained in all publications are solely those of the individual author(s) and contributor(s) and not of MDPI and/or the editor(s). MDPI and/or the editor(s) disclaim responsibility for any injury to people or property resulting from any ideas, methods, instructions or products referred to in the content.